

# Instrumented cardiac microphysiological devices via multimaterial three-dimensional printing

Johan U. Lind<sup>1,2†</sup>, Travis A. Busbee<sup>1,2†</sup>, Alexander D. Valentine<sup>1,2</sup>, Francesco S. Pasqualini<sup>1,2</sup>, Hongyan Yuan<sup>1,2‡</sup>, Moran Yadid<sup>1,2</sup>, Sung-Jin Park<sup>1,2</sup>, Arda Kotikian<sup>1,2</sup>, Alexander P. Nesmith<sup>1,2</sup>, Patrick H. Campbell<sup>1,2</sup>, Joost J. Vlassak<sup>2</sup>, Jennifer A. Lewis<sup>1,2\*</sup> and Kevin K. Parker<sup>1,2\*</sup>

**Biomedical research has relied on animal studies and conventional cell cultures for decades. Recently, microphysiological systems (MPS), also known as organs-on-chips, that recapitulate the structure and function of native tissues *in vitro*, have emerged as a promising alternative<sup>1</sup>. However, current MPS typically lack integrated sensors and their fabrication requires multi-step lithographic processes<sup>2</sup>. Here, we introduce a facile route for fabricating a new class of instrumented cardiac microphysiological devices via multimaterial three-dimensional (3D) printing. Specifically, we designed six functional inks, based on piezo-resistive, high-conductance, and biocompatible soft materials that enable integration of soft strain gauge sensors within micro-architectures that guide the self-assembly of physio-mimetic laminar cardiac tissues. We validated that these embedded sensors provide non-invasive, electronic readouts of tissue contractile stresses inside cell incubator environments. We further applied these devices to study drug responses, as well as the contractile development of human stem cell-derived laminar cardiac tissues over four weeks.**

Current MPS models of muscle tissue rely on microscopy coupled with optical tracking analysis for assessing tissue contractile stress. For instance, muscular thin-film (MTF) assays track changes in curvature of soft cantilever substrates induced by the contraction of a laminar tissue<sup>3</sup>, and micro-post assays measure the deflection of pillars supporting a micro-tissue<sup>4</sup>. Although these assays have proved valuable for short-term modelling of human disease and small-scale drug screening applications<sup>1,5,6</sup>, they are not well suited for higher-throughput or longer-term studies. Moreover, biomimetic microsystems are at present fabricated using soft material lithography-based techniques that require multiple steps, masks and dedicated tools<sup>4,7–9</sup>, which hinders rapid prototyping and customization. By contrast, multimaterial 3D printing of viscoelastic inks enables a wide range of functional, structural and biological materials to be patterned and integrated in a single programmable manufacturing step<sup>10–14</sup>.

Here, we introduce a fully 3D printed and instrumented microphysiological device that provides continuous electronic readout of the contractile stress of multiple laminar cardiac micro-tissues (Fig. 1a,b). Each device contains three key features: multilayer cantilevers, composed of a base layer, an embedded strain sensor, and a tissue-guiding layer; electrical interconnects for readout; and eight independent wells (Fig. 1c–i). The tissue-guiding layer promotes self-assembly of engineered physio-mimetic laminar tissues from

neonatal rat ventricular myocytes (NRVMs) and human induced pluripotent stem cell-derived cardiomyocytes (hiPS-CMs). Our microphysiological device facilitates tissue culture and non-invasive analyses of tissue contractile strength over several weeks, and facilitates drug studies inside a controlled incubator environment.

To create this integrated device, six materials are patterned sequentially via direct ink writing multimaterial 3D printing. To allow material integration at the microscale, the substrate topology and  $x$ – $y$ – $z$  positions of four individually addressable nozzles are determined by an automated calibration process (see Supplementary Movie 1). After this calibration, the device is printed in a single continuous procedure (Fig. 1c–i and Supplementary Movies 2 and 3).

The stress generated by laminar cardiac tissues is limited to the range 1–15 kPa (refs 5,8). Hence, to match this range, both the thickness and stiffness of each cantilever layer must be minimized. Towards this objective, we designed a series of highly dilute polymer-based inks. Their low solids content ensures patterning of thin individual layers (0.5–6.5  $\mu\text{m}$  in thickness). Additionally, by tuning the evaporation rate of the carrier solvent solution, the ink viscosity and corresponding wetting and spreading behaviour is controlled to achieve the desired lateral dimensions (Supplementary Figs 1 and 2). Using these inks, 0.5  $\mu\text{m}$  dextran films are printed first (Fig. 1c). These serve as biocompatible, water-soluble sacrificial release layers that allow the final cantilevers to detach from the substrate and deflect freely. Next, using dilute thermoplastic polyurethane (TPU) inks, 3- $\mu\text{m}$ -thick cantilever bases, 6.5- $\mu\text{m}$ -thick strain gauge wires and 1.5- $\mu\text{m}$ -thick wire covers are printed in steps 2–4, respectively (Fig. 1d–f). The cantilever base and wire covers are printed using an unfilled TPU ink, whereas the strain gauge wires are printed using a TPU ink filled with 25 wt% carbon black nanoparticles (CB:TPU). The printed TPU-based features exhibit elastic mechanical properties with a Young's modulus of 1.6 MPa (Supplementary Fig. 3), whereas CB:TPU features readily cure to form an elastic piezo-resistive material with a Young's modulus of 8.8 MPa and resistivity of 1.19  $\Omega\text{ cm}$  (Supplementary Figs 3–7). Several alternative fillers were investigated, including metals particles<sup>15</sup> and carbon nanotubes<sup>16</sup>. However, we found that carbon black imparts the best combination of ink rheology, low stiffness and sensor hysteresis.

The remainder of the microphysiological device is printed using concentrated viscoelastic inks optimized for deposition of self-supporting structures (Supplementary Figs 8 and 9). Using a

<sup>1</sup>Wyss Institute for Biologically Inspired Engineering, Harvard University, Boston, Massachusetts 02115, USA. <sup>2</sup>John A. Paulson School of Engineering and Applied Sciences, Harvard University, Cambridge, Massachusetts 02138, USA. <sup>†</sup>These authors contributed equally to this work. <sup>‡</sup>Present address: Department of Mechanical, Industrial and Systems Engineering, University of Rhode Island, Kingston, Rhode Island 02881, USA.

\*e-mail: jalewis@seas.harvard.edu; kkparker@seas.harvard.edu

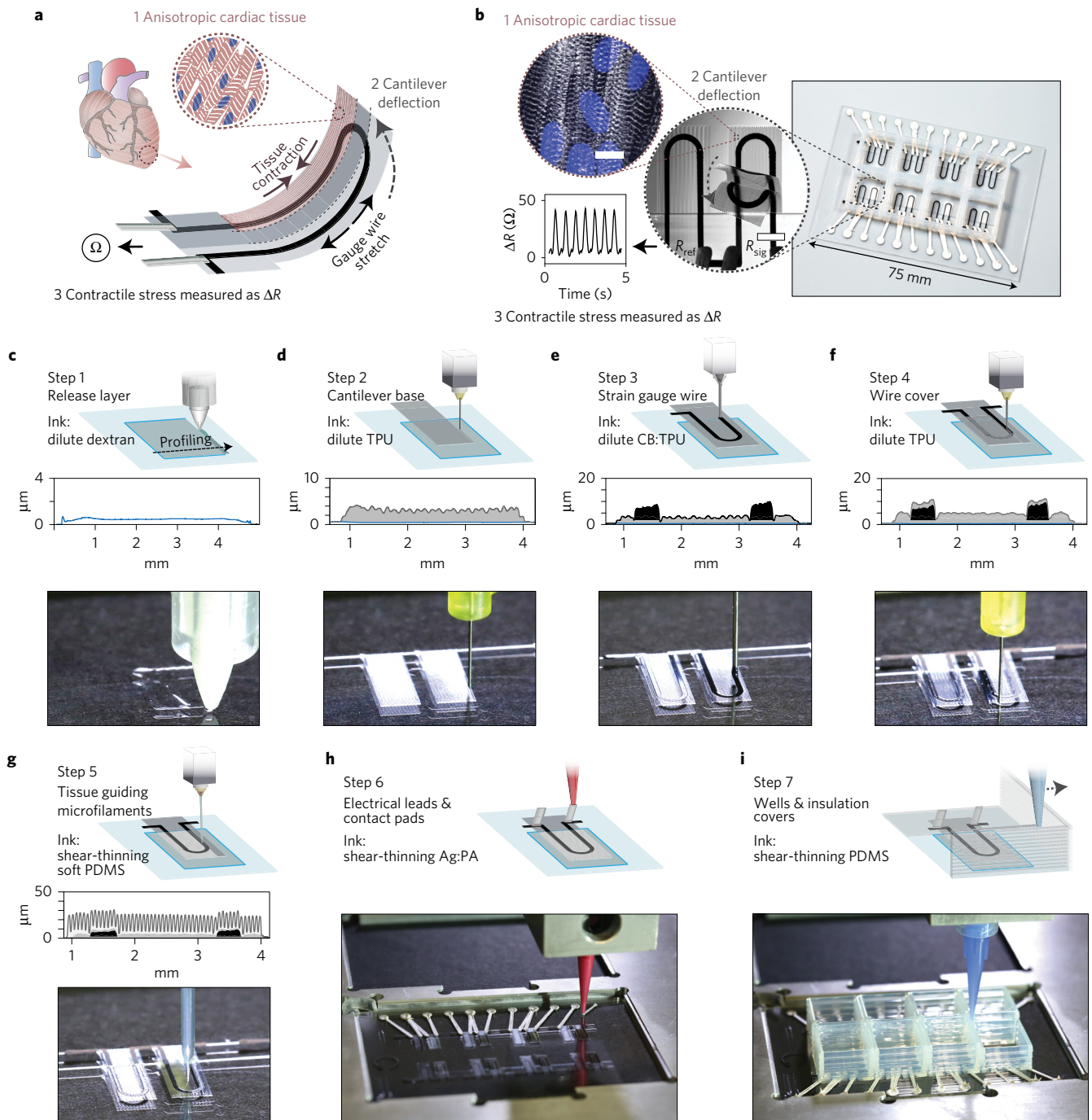


**Figure 1 | Device principle and microscale 3D-printing procedure.** **a**, Sketch of the device principle. Contraction of an anisotropic engineered cardiac tissue (1) deflects a cantilever substrate (2), thereby stretching a soft strain gauge embedded in the cantilever. This generates a resistance change proportional to the contractile stress of the tissue (3). **b**, The fully printed final device. Insert 1: Confocal microscopy image of immunostained laminar NRVM cardiac tissue on the cantilever surface. Blue, DAPI nuclei stain. White,  $\alpha$ -actinin. Scale bar, 10  $\mu\text{m}$ . Insert 2: Still images of a cantilever deflecting upon tissue contraction. Insert 3: Example resistance signal. **c–i**, Automated printing of the device on a 2 inch  $\times$  3 inch glass slide substrate in seven sequential steps. For each step, a corresponding still image from the printing procedure is shown. For steps 1–5, a stylus profiling cross-sectional contour of the cantilever is also shown. **c**, In print step 1, a 0.5- $\mu\text{m}$  dextran thin-film sacrificial layer is printed. **d**, In print step 2, a 3  $\mu\text{m}$  TPU thin-film cantilever base is printed. **e**, In print step 3, a 6.5- $\mu\text{m}$ -thick CB:TPU strain sensor loop is added to the cantilever base. **f**, In print step 4, a 1.5- $\mu\text{m}$  TPU wire cover is added. **g**, In print step 5, 20- $\mu\text{m}$ -tall, 60- $\mu\text{m}$ -wide PDMS microfilaments are printed in slightly overlapping lines. The filaments constitute the top part of the cantilever and guide cardiomyocytes to form anisotropic laminar tissues. **h**, In print step 6, electrical leads and contact are added using a high-conductivity Ag:PA ink. **i**, In print step 7, covers to insulate exposed wires and wells to contain cells and media are printed using PDMS, PLA or ABS (see Supplementary Fig. 10).

viscous polydimethylsiloxane (PDMS) ink (Young's modulus of 1.28 MPa, see Supplementary Fig. 3),  $\sim$ 60- $\mu\text{m}$ -wide filaments are patterned on top of each cantilever (Fig. 1g). These comprise the majority of the cantilever thickness and serve as direct support

below the physio-mimetic laminar cardiac tissue. Next, electrical leads and contact pads are printed using a high-conductivity, silver particle-filled, polyamide (Ag:PA) ink (Fig. 1h). Upon drying, the printed wires exhibit an electrical resistivity of  $6.6 \times 10^{-3} \Omega \text{cm}$

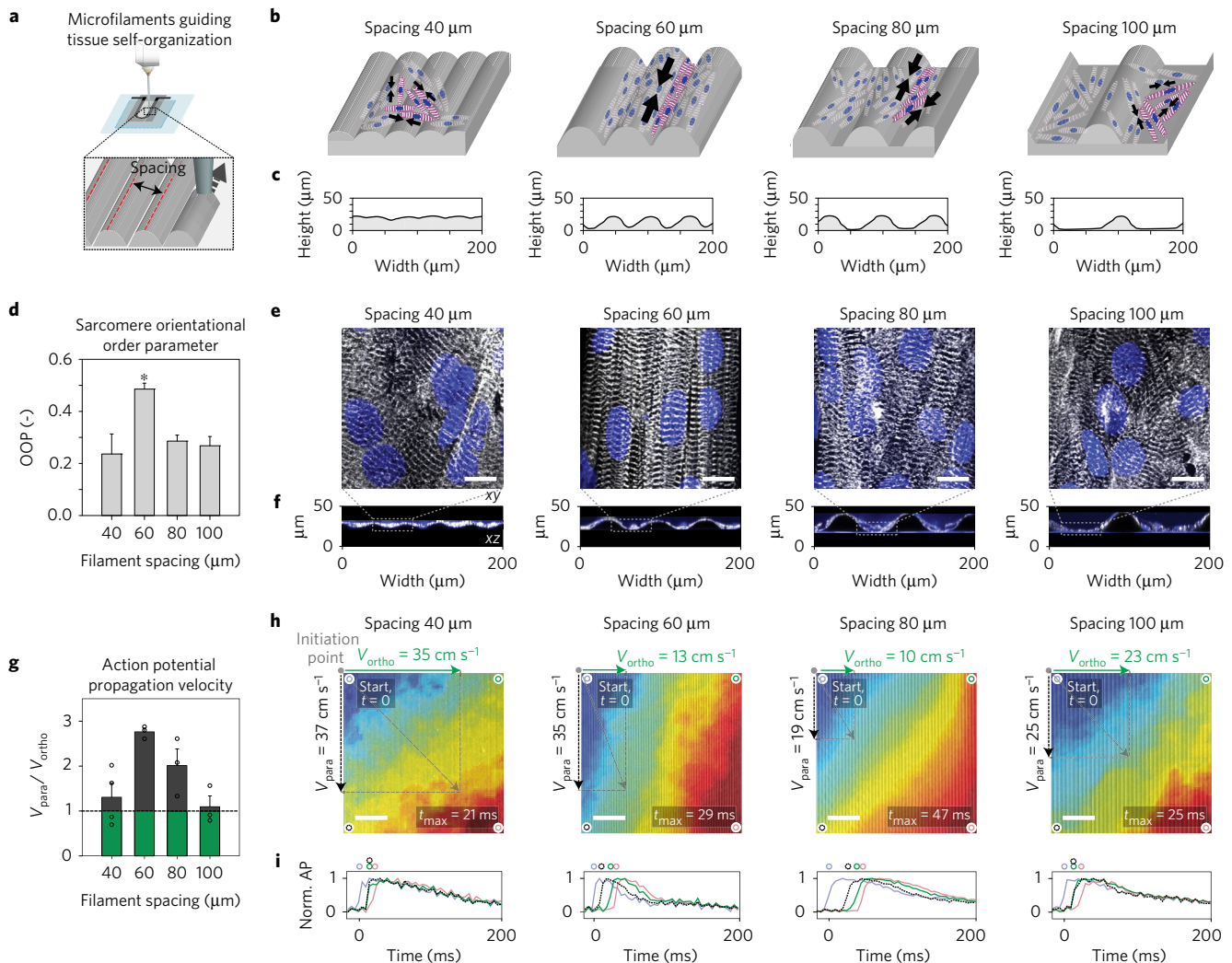


**Figure 2 | Micro-grooves guide cardiomyocyte self-assembly into anisotropic engineered tissues.** **a**, Spacing of soft PDMS microfilaments. **b**, Sketch of microfilaments guiding self-assembly of engineered cardiac tissue. **c**, Stylus profilometer contours of substrates with filaments printed at 40, 60, 80 and 100  $\mu\text{m}$  spacing. **d**, Sarcomere OOP of laminar NRVM tissues developed on substrates with 40 ( $n=9$ ), 60 ( $n=13$ ), 80 ( $n=8$ ) and 100  $\mu\text{m}$  ( $n=10$ ) filament spacing. Error bars are standard error of the mean (s.e.m.),  $*$ ,  $P < 0.05$ . **e, f**, Representative confocal images from OOP data set z-projection (**e**) and x-z line scan (**f**). Blue, DAPI nuclei stain. White,  $\alpha$ -actinin. Scale bars, 10  $\mu\text{m}$ . **g**, Ratio between action potential (AP) propagation speed parallel and orthogonal to the grooves for laminar NRVM tissue developed on substrates with 40, 60, 80 and 100  $\mu\text{m}$  filament spacing, ( $n \geq 3$ ). Individual data points included (circles). Error bars are s.e.m. **h**, Representative activation time heat maps for AP data set, overlaid with wide-field microscope image of the samples as guide to the eye. Scale bars, 0.8 mm. Activation times normalized to maximum observed activation ( $t_{\text{max}}$ , red), to account for tissue source variation. 2 Hz electrical point stimulation is applied in top-left corner of samples. Mean observed propagation speed parallel ( $V_{\text{para}}$ ) and orthogonal ( $V_{\text{ortho}}$ ) to grooves is shown as vectors. **i**, Normalized AP traces at four corners of activation map samples. Blue, at AP initiation corner. Red, at  $t_{\text{max}}$ -corner. Black, corner parallel to grooves. Green, corner orthogonal to grooves.

(Supplementary Fig. 4), which ensures that the primary electrical resistance of the final device arises from the embedded CB:TPU strain gauges. Finally, the wire leads are covered with an insulating layer, and eight individually addressable wells are printed using either a PDMS ink or biocompatible rigid thermoplastic polymers such as polylactic acid (PLA) or acrylonitrile butadiene styrene (ABS). The rigid polymers can be preferable for drug study applications, as they are less prone to bulk absorption of hydrophobic drugs than PDMS<sup>17</sup> (Fig. 1i and Supplementary Fig. 10). After printing, the devices are cured at 100 °C and subsequently seeded with cardiomyocytes, which self-assemble into laminar tissues mimicking the structure of the native heart.

The musculature of the heart is composed of highly organized, structurally and electrically anisotropic layers<sup>18</sup>. To recapitulate this architecture *in vitro*, we printed a range of grooved microstructures by varying the spacing between curved  $\sim 20 \mu\text{m} \times 60 \mu\text{m}$

(height  $\times$  width) filaments and assessed their ability to guide the self-assembly of anisotropic laminar NRVM tissues (Fig. 2). We evaluated the degree of tissue structural anisotropy using immunofluorescent imaging of sarcomeric  $\alpha$ -actinin and quantification of the sarcomere orientational order parameter (OOP) (Fig. 2a–f and Supplementary Fig. 11)<sup>19</sup>. All substrates showed an OOP  $> 0.2$ , indicative of nonrandom sarcomere alignment. The highest OOP  $\sim 0.5$  was observed for a 60  $\mu\text{m}$  filament spacing. Similarly, a 60  $\mu\text{m}$  filament spacing gave rise to the highest degree of electrophysiological anisotropy in the laminar NRVM tissues (Fig. 2g–i and Supplementary Movies 4–7). For this spacing, action potential propagation was 2.7 times faster parallel to the grooves compared to the transverse direction. These data are in agreement with the longitudinal to transverse velocity ratio of 2.1 observed in the native ventricle<sup>18</sup>. Also, these anisotropic laminar tissues gave rise to unidirectional and concerted cantilever deflection and exhibited the highest

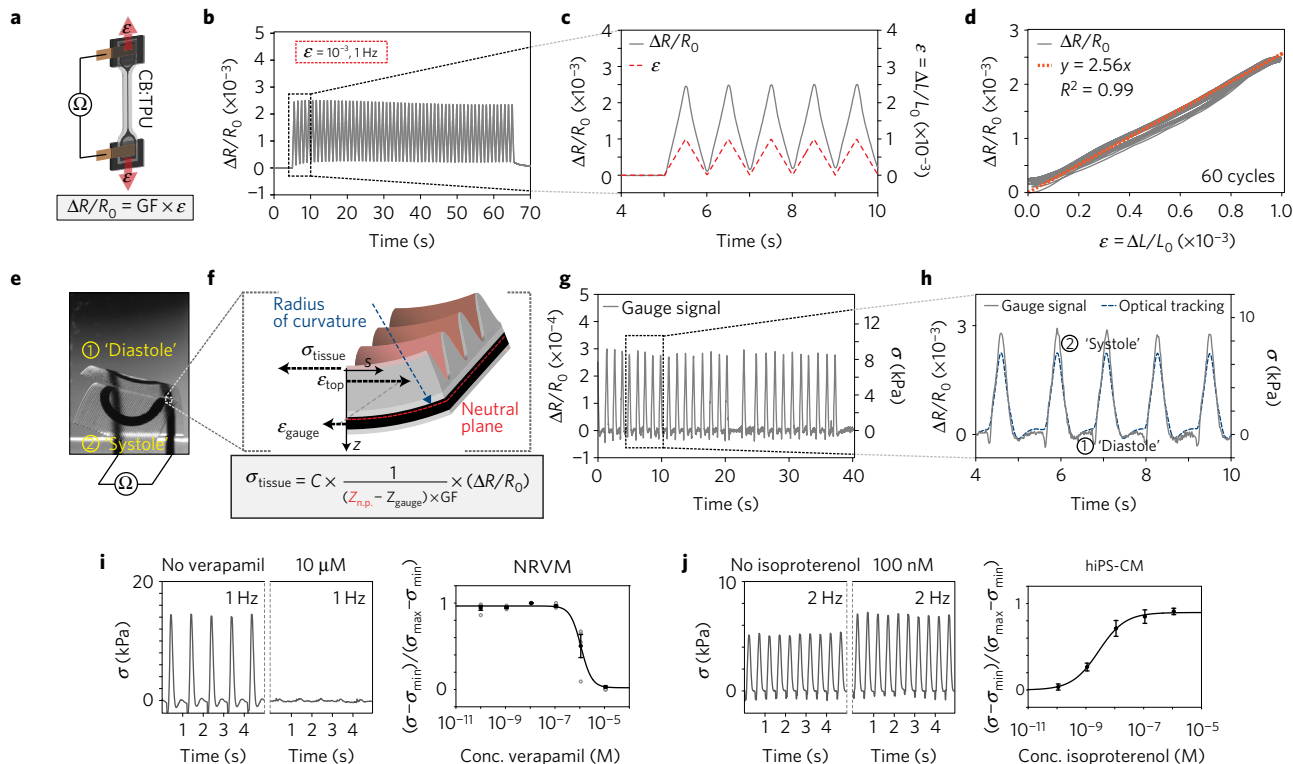


**Figure 3 | CB:TPO gauge factor, sensor readout and example drug-dose studies.** **a**, Sketch of Instron test set-up for determining CB:TPO gauge factor (GF). **b–d**, Relative change in CB:TPO resistance upon triangular cyclic straining to 0.1% at 1 Hz. In **c** the dark grey line is the observed relative resistance change and the red dotted line is the strain applied. **d**, Relative resistance change versus applied strain. Orange dotted line indicates a linear fit to part of the cycles with increasing strain, yielding a gauge factor of 2.56. **e**, Wide-field microscope images of cantilever bending upon tissue contraction. Minimum deflection corresponds to cardiac diastole (1) and peak deflection corresponding to systole (2). **f**, Sketch of the mechanical model used to convert change in gauge resistance to stress generated by the tissue, through a linear conversion factor C as described in Supplementary Information. **g,h**, Relative resistance changes (left axis) and corresponding calculated tissue twitch stress (right axis) recorded from spontaneously beating cantilever. The blue dotted line in **h** indicates stress determined independently by optical tracking of the cantilever radius of curvature. **i**, Representative traces of twitch stress generated by a laminar NRVM tissue when tissue is exposed to verapamil and corresponding dose–response curve ( $n = 4$ ). Error bars are s.e.m., stress normalized between maximal and minimal values, tissue paced at 1 Hz, apparent  $EC_{50} 1.12 \times 10^{-6}$  M. Individual data points included (circles). **j**, Representative traces of twitch stress generated by a laminar hiPS-CM tissue when exposed to isoproterenol and corresponding dose–response curve, ( $n = 10$ ). Error bars are s.e.m., stress normalized between maximal and minimal values, tissue paced at 2 Hz, apparent  $EC_{50} 2.74 \times 10^{-9}$  M.

contractile stresses in the final devices (Supplementary Figs 12–14). Collectively, these results demonstrate that our printing technique can be employed to engineer laminar cardiac tissues with a range of ordered architectures. Notably, the OOP and electrophysiology data closely matched values obtained using semi-manual micro-contact printing and moulding techniques<sup>7,20,21</sup>.

To accurately measure the stress exerted by the physio-mimetic laminar cardiac tissues, the embedded strain gauges within each cantilever must produce a reliable and detectable signal. We therefore evaluated the electro-mechanical properties of CB:TPO in a series of uniaxial strain tests (Fig. 3a–d and Supplementary Figs 5–7). To mimic the strains exerted by tissue contraction, 1–3 Hz triangular strains of 0.1% were applied to CB:TPO gauges. In this strain range, the gauges exhibited a linear strain–resistance relationship with limited hysteresis and a corresponding gauge factor of  $2.51 \pm 0.09$ . In order to accurately convert resistance signals to stresses generated by the laminar cardiac tissues, we established a mechanical model of the cantilevers based on a multilayer version of Stoney’s equation (Fig. 3e,f and Supplementary Information). The mechanical model relies on the dimensions and Young’s moduli of each layer of the cantilever as well as the CB:TPO gauge factor. The model provides linear conversion factors between the relative changes in gauge resistance, changes in cantilever radius of curvature and, in turn, the longitudinal stresses generated by the laminar cardiac tissues. Applying these conversion factors,

we obtained tissue twitch stress ( $\sigma$ ), the differences between the systolic and diastolic stress, in the range of 7–15 kPa for laminar NRVM tissues, akin to prior reports<sup>3,7</sup>. To further verify the model, we compared the sensor readout with stress values concurrently obtained through optical tracking of cantilever deflection, and obtained highly similar stress values (Fig. 3g,h and Supplementary Figs 12 and 13 and Supplementary Movies 8–11). However, we observed one discrepancy between the optical tracking and electrical readout: at the initiation of tissue contraction, a small decrease in gauge resistance is seen, prior to the increase caused by cantilever deflection. We attribute this decrease to a brief axial compression of the gauge wire occurring during initial tissue contraction, while cantilever deflection is counteracted by inertial and viscous forces. Notably, this observation does not influence tissue twitch stress values. Together, these results demonstrate that the CB:TPO strain gauges embedded in our fully printed platform provide reliable readouts of tissue contractile stress.

Data acquisition from cardiac microphysiological systems based on optical readout is laborious, requires dedicated microscopy set-ups and semi-automated image analysis software, and is limited by the image readout file sizes<sup>4,5</sup>. By contrast, our fully printed and instrumented cardiac devices provide a direct non-invasive electronic readout of contractile stresses. Therefore, we could perform dose–response studies of drugs that influence contraction strength or beat rate directly inside a cell incubator, an ideal *in vitro* environment

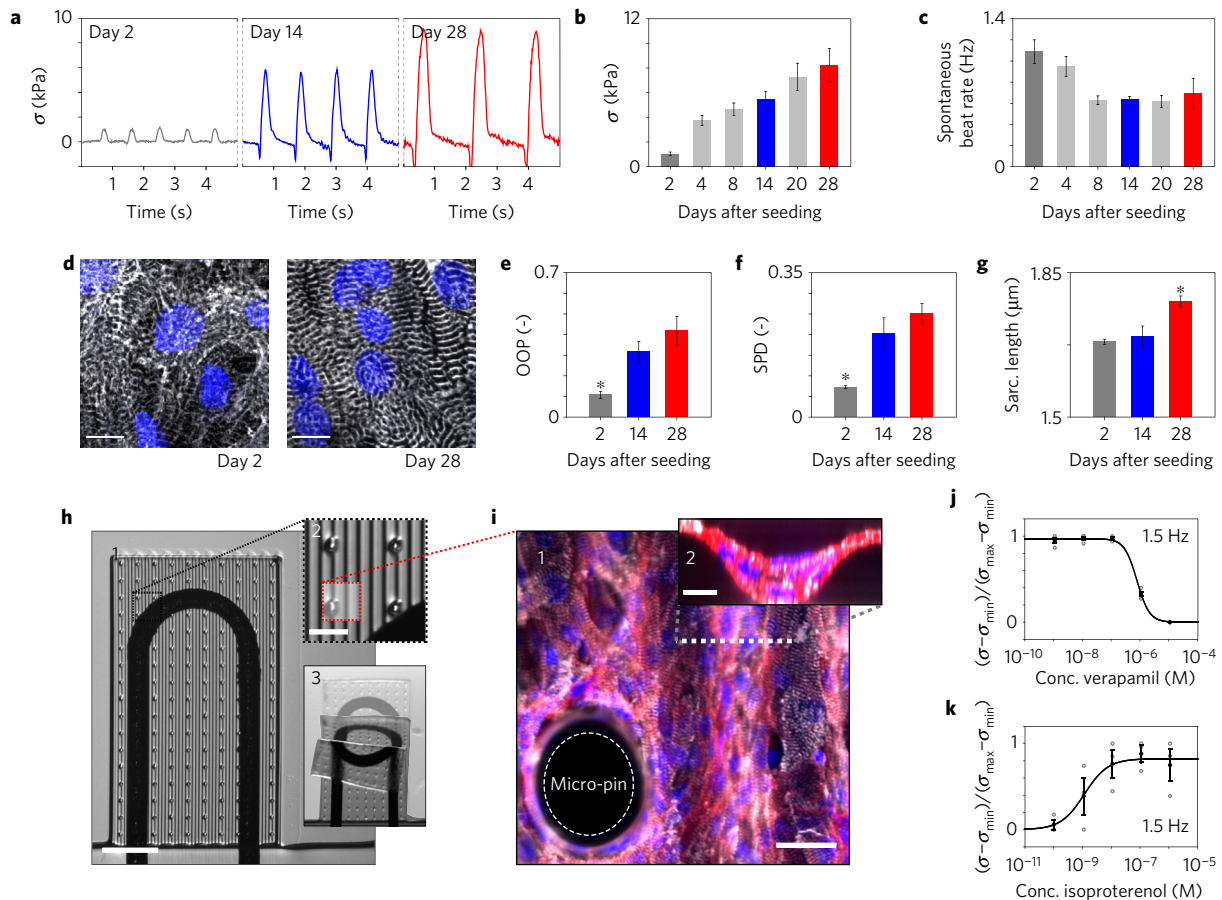


**Figure 4 | Long-term hiPS-CM contractile development and thicker laminar NRVM tissue devices.** **a**, Representative traces of contractile twitch stress generated by the laminar hiPS-CMs tissues at day 2, 14 and 28. **b, c**, Contractile stress and spontaneous beat rate of hiPS-CMs tissues at day 2, 4, 8, 20 and 28 ( $n \geq 10$ ). Error bars are s.e.m. **d**, Immunostained laminar hiPS-CMs tissues on device cantilevers at day 2 and day 28 after seeding. Scale bars 10  $\mu\text{m}$ . Blue: DAPI nuclei stain. White:  $\alpha$ -actinin stain, z-projection. **e-g**, SPD, OOP and sarcomere length of laminar hiPS-CM tissues at day 2, 14 and 28 ( $n = 5$ ). Error bars are s.e.m., \*,  $P < 0.05$ . **h**, 1: Modified device cantilever containing micro-pin and micro-well to support thicker laminar NRVM tissue. 2: Detail of cantilever with micro-pins. 3: Still images of a cantilever deflecting upon tissue contraction. **i**, 1: z-projection of immunostained thicker laminar tissue on the cantilever surface with micro-pin (scale bar, 30  $\mu\text{m}$ ). 2: x-z line scan of thicker laminar tissue in grooves (scale bar, 10  $\mu\text{m}$ ). Blue, DAPI nuclei stain. White,  $\alpha$ -actinin. Red, actin. **j, k**, Dose-response curves for thicker laminar NRVM tissues. Stress values for thicker tissues assumed linear proportional to relative resistance change:  $\sigma \sim \Delta R/R_0$ . Stress normalized between maximal and minimal values. **j**, Dose-response curve for verapamil ( $n = 4$ ). Error bars are s.e.m. Individual data points included (circles), tissue paced at 1.5 Hz. Apparent  $\text{EC}_{50}$   $7.90 \times 10^{-7}$  M. **k**, Dose-response curve for isoproterenol ( $n = 3$ ). Error bars are s.e.m. Individual data points included (circles), tissue paced at 1.5 Hz. Apparent  $\text{EC}_{50}$   $1.16 \times 10^{-9}$  M.

(Fig. 3i, j and Supplementary Figs 15–18). As examples, we carried out cumulative drug-dose studies with the L-type calcium channel blocker verapamil and the  $\beta$ -adrenergic agonist isoproterenol. For laminar NRVM tissues we observed a negative inotropic response to verapamil, with an apparent  $\text{EC}_{50}$  of  $1.15 \times 10^{-6}$  M when paced at 1 Hz (Fig. 3i). We also observed a negative chronotropic effect for spontaneously beating tissues (Supplementary Fig. 17), in good agreement with prior studies on isolated postnatal whole rat hearts<sup>25</sup>. Similarly, we observed a positive chronotropic response to isoproterenol for spontaneously beating laminar tissues, matching previous studies of engineered NRVM micro-tissues<sup>4</sup> (Supplementary Fig. 18). For hiPS-CM-based laminar tissues, we observed a positive inotropic response to isoproterenol, with an apparent  $\text{EC}_{50}$  of  $2.69 \times 10^{-9}$  M when paced at 2 Hz (Fig. 3j), resembling studies based on embryonic stem cell-derived cardiomyocyte tissue<sup>23</sup>.

Beyond facilitating acute drug studies, our platform is well suited for extended studies to identify gradual changes in the contractile stress of engineered cardiac tissues, which can occur over the course of multiple weeks<sup>23,24</sup>. As a demonstration, we studied the *in vitro* contractile development of laminar tissues based on hiPS-CMs over the course of 28 days (Fig. 4a–g). During this

period, the longitudinal contractile stress initially increased by a factor of four from day 2 to 4, followed by a more gradual increase (Fig. 4a, b). Similarly, the spontaneous beating rate decreased (Fig. 4c), indicative of increased maturity<sup>25</sup>. The changes in twitch stress are mirrored by a structural development of the laminar hiPS-CM tissues (Fig. 4d–g and Supplementary Figs 19 and 20). From day 2 to day 14 the sarcomere OOP increased from 0.11 to 0.32 (Fig. 4e), while the sarcomere packing density (SPD, a measure of sarcomere periodic organization) increased from 0.07 to 0.2 (Fig. 4f), indicating that hiPS-CMs undergo sarcomerogenesis and myofibrillogenesis during culture<sup>19</sup>. Importantly, from day 14 to day 28, a significant increase in sarcomere length from 1.7  $\mu\text{m}$  to 1.8  $\mu\text{m}$  was observed (Fig. 4g), indicative of a more mature tissue<sup>26</sup>.

Although traditional muscular thin films mimic essential features of the cardiac architecture, cell–cell contacts are confined to a single cell layer. By contrast, a number of *in vitro* cardiac tissue models composed of thicker micro-tissues have been reported<sup>24,27–29</sup>. To illustrate the versatility of our 3D-printing methodology, we modified the MPS device to support thicker micro-tissues, approximately four cell layers in thickness (Supplementary Figs 21–24). This thickness matches that of the myocyte layers in a mammalian

heart (that is,  $\sim 4$  cells in thickness per layer, each layer separated by connective tissue)<sup>30</sup>. To balance the increased contractile stress and mitigate tissue delamination, we printed thicker cantilevers that contained  $\sim 100\text{-}\mu\text{m}$ -tall micro-pin arrays with tunable areal density (Fig. 4h,i and Supplementary Movies 13–15). Despite these modifications to both the cardiac tissue and cantilevers, the tissue remains orders of magnitude softer than the substrate. Hence, the basic assumptions of the mechanical model remain valid, and the sensor signal is directly proportional to mean tissue stress (see Supplementary Information). We carried out proof-of-principle isoproterenol and verapamil drug studies to illustrate the functional relevance of these thicker NRVM-based tissues (Fig. 4j,k). We observed the expected positive and negative inotropic responses with apparent EC<sub>50</sub> values comparable to earlier data from engineered 3D NRVM tissues and isolated postnatal whole rat hearts<sup>22,29</sup>.

Through multimaterial 3D printing of a series of customized inks, we demonstrated the automated design and fabrication of instrumented cardiac microphysiological devices. The integrated sensors drastically simplify data acquisition and long-term functional studies. Leveraging the ability to track the temporal development in tissue mechanics will enable new insights into tissue morphogenesis, pathogenesis, and drug-induced structural and functional remodelling. Our digital manufacturing approach is versatile, allowing for fabrication of a range of instrumented microphysiological devices. Notably, our approach facilitates rapid customization to match device geometries, mechanical and biochemical properties to a specific diseased state or a unique patient-derived cell source. Our programmable microfabrication approach opens new avenues for *in vitro* tissue engineering, toxicology and drug screening research.

## Methods

Methods and any associated references are available in the [online version of the paper](#).

Received 21 January 2016; accepted 23 September 2016;  
published online 24 October 2016

## References

- Bhatia, S. N. & Ingber, D. E. Microfluidic organs-on-chips. *Nat. Biotechnol.* **32**, 760–772 (2014).
- Mammoto, A. *et al.* Control of lung vascular permeability and endotoxin-induced pulmonary oedema by changes in extracellular matrix mechanics. *Nat. Commun.* **4**, 1759 (2013).
- Feinberg, A. W. *et al.* Muscular thin films for building actuators and powering devices. *Science* **317**, 1366–1370 (2007).
- Boudou, T. *et al.* A microfabricated platform to measure and manipulate the mechanics of engineered cardiac microtissues. *Tissue Eng. A* **18**, 910–919 (2011).
- Wang, G. *et al.* Modeling the mitochondrial cardiomyopathy of Barth syndrome with induced pluripotent stem cell and heart-on-chip technologies. *Nat. Med.* **20**, 616–623 (2014).
- Hinson, J. T. *et al.* Titin mutations in iPSCs define sarcomere insufficiency as a cause of dilated cardiomyopathy. *Science* **349**, 982–986 (2015).
- Agarwal, A. *et al.* Micropatterning alginate substrates for *in vitro* cardiovascular muscle on a chip. *Adv. Funct. Mater.* **23**, 3738–3746 (2013).
- Grosberg, A., Alford, P. W., McCain, M. L. & Parker, K. K. Ensembles of engineered cardiac tissues for physiological and pharmacological study: heart on a chip. *Lab Chip* **11**, 4165–4173 (2011).
- Park, S.-J. *et al.* Phototactic guidance of a tissue-engineered soft-robotic ray. *Science* **353**, 158–162 (2016).
- Lewis, J. A. Direct ink writing of 3D functional materials. *Adv. Funct. Mater.* **16**, 2193–2204 (2006).
- Hardin, J. O., Ober, T. J., Valentine, A. D. & Lewis, J. A. Microfluidic printheads for multimaterial 3D printing of viscoelastic inks. *Adv. Mater.* **27**, 3279–3284 (2015).
- Sun, K. *et al.* 3D printing of interdigitated Li-Ion microbattery architectures. *Adv. Mater.* **25**, 4539–4543 (2013).
- Miller, J. S. *et al.* Rapid casting of patterned vascular networks for perfusable engineered three-dimensional tissues. *Nat. Mater.* **11**, 768–774 (2012).
- Kolesky, D. B., Homan, K. A., Skylar-Scott, M. A. & Lewis, J. A. Three-dimensional bioprinting of thick vascularized tissues. *Proc. Natl Acad. Sci. USA* **113**, 3179–3184 (2016).
- Matsuhisa, N. *et al.* Printable elastic conductors with a high conductivity for electronic textile applications. *Nat. Commun.* **6**, 7461 (2015).
- Lipomi, D. J. *et al.* Skin-like pressure and strain sensors based on transparent elastic films of carbon nanotubes. *Nat. Nanotech.* **6**, 788–792 (2011).
- Berthier, E., Young, E. W. & Beebe, D. Engineers are from PDMS-land, biologists are from polystyrenia. *Lab Chip* **12**, 1224–1237 (2012).
- Kl eber, A. G. & Rudy, Y. Basic mechanisms of cardiac impulse propagation and associated arrhythmias. *Physiol. Rev.* **84**, 431–488 (2004).
- Pasqualini, F. S., Sheehy, S. P., Agarwal, A., Aratyn-Schaus, Y. & Parker, K. K. Structural phenotyping of stem cell-derived cardiomyocytes. *Stem Cell Rep.* **4**, 340–347 (2015).
- Feinberg, A. W. *et al.* Controlling the contractile strength of engineered cardiac muscle by hierarchical tissue architecture. *Biomaterials* **33**, 5732–5741 (2012).
- Sheehy, S. P. *et al.* Quality metrics for stem cell-derived cardiac myocytes. *Stem Cell Rep.* **2**, 282–294 (2014).
- O stf adlov a, I. *et al.* Early postnatal development of contractile performance and responsiveness to Ca<sup>2+</sup>, verapamil and ryanodine in the isolated rat heart. *J. Mol. Cell. Cardiol.* **25**, 733–740 (1993).
- Zhang, D. *et al.* Tissue-engineered cardiac patch for advanced functional maturation of human ESC-derived cardiomyocytes. *Biomaterials* **34**, 5813–5820 (2013).
- Zimmermann, W. H. *et al.* Three-dimensional engineered heart tissue from neonatal rat cardiac myocytes. *Biotechnol. Bioeng.* **68**, 106–114 (2000).
- Reiser, P. J., Portman, M. A., Ning, X.-H. & Moravec, C. S. Human cardiac myosin heavy chain isoforms in fetal and failing adult atria and ventricles. *Am. J. Physiol.* **280**, H1814–H1820 (2001).
- Lundy, S. D., Zhu, W.-Z., Regnier, M. & Laflamme, M. A. Structural and functional maturation of cardiomyocytes derived from human pluripotent stem cells. *Stem Cells Dev.* **22**, 1991–2002 (2013).
- Nunes, S. S. *et al.* Biowire: a platform for maturation of human pluripotent stem cell-derived cardiomyocytes. *Nat. Methods* **10**, 781–787 (2013).
- Xiao, Y. *et al.* Microfabricated perfusable cardiac biowire: a platform that mimics native cardiac bundle. *Lab Chip* **14**, 869–882 (2014).
- Zimmermann, W.-H. *et al.* Tissue engineering of a differentiated cardiac muscle construct. *Circ. Res.* **90**, 223–230 (2002).
- LeGrice, I. J. *et al.* Laminar structure of the heart: ventricular myocyte arrangement and connective tissue architecture in the dog. *Am. J. Physiol.* **269**, H571–H582 (1995).

## Acknowledgements

The authors thank L. K. Sanders for her work on photography and time-lapse movies, J. A. Goss for his assistance with fabrication of the device holder and J. Minardi for his development of Mecode, and his help with machine automation. This work was performed in part at the Center for Nanoscale Systems (CNS), a member of the National Nanotechnology Infrastructure Network (NNIN), which is supported by the National Science Foundation under NSF award no. ECS-0335765. CNS is part of Harvard University. This work was also supported by the National Center For Advancing Translational Sciences of the National Institutes of Health under Award Number UH3TR000522, the US Army Research Laboratory and the US Army Research Office under Contract No. W911NF-12-2-0036, the Air Force Research Laboratory under Contract No. FA8650-09-D-5037-0004, and the Harvard University Materials Research Science and Engineering Center (MRSEC) award no. DMR-1420570. J.U.L. gratefully acknowledges support from the Villum Foundation. J.A.L. gratefully acknowledges support from the Office of Naval Research, Vannevar Bush National Security Science and Engineering Faculty Fellowship (Award No. N00014-16-1-2823).

## Author contributions

J.U.L., T.A.B., J.A.L. and K.K.P. designed the study. J.U.L. and T.A.B. designed the device. T.A.B. coded the 3D-print procedure and automation. J.U.L., T.A.B., A.K. and A.D.V. developed and characterized the printable materials. J.U.L., A.D.V. and T.A.B., optimized and printed devices. P.H.C. performed NRVM harvesting and prepared culturing media. J.U.L., M.Y. and A.P.N. performed NRVM culture, drug-dose experiments, and data analysis. M.Y. and J.U.L. conducted hiPS-CM culture, experiments and data analysis. F.S.P. and J.U.L. performed tissue staining, confocal imaging, and OOP analysis. S.-J.P. and J.U.L. conducted optical mapping experiments and analysis. H.Y. and J.J.V. developed the mechanical model of the device. J.U.L., T.A.B., J.A.L. and K.K.P. prepared illustrations and wrote the manuscript. F.S.P. and A.D.V. contributed to writing the manuscript.

## Additional information

Supplementary information is available in the [online version of the paper](#). Reprints and permissions information is available online at [www.nature.com/reprints](http://www.nature.com/reprints). Correspondence and requests for materials should be addressed to J.A.L. or K.K.P.

## Competing financial interests

The authors declare no competing financial interests.

## Methods

**Ink formulations.** The following ink formulations were used: dextran ink: 10 g ml<sup>-1</sup> dextran (Sigma-Aldrich) was dissolved in 75:25 v:v, water: isopropanol. TPU ink: TPU 15 wt% Elastollan 35A (BASF) dissolved in 4:1 v:v tetrahydrofuran:dimethylformamide. CB:TPU ink: TPU 15 wt% Elastollan 35A, 5 wt% carbon black (Vulcan XC72R, Cabot) dissolved in 4:1 v:v tetrahydrofuran:dimethylformamide. Ag:Pa ink: 50 g silver flakes (5–8 μm) mixed with 5.2 g 30 wt% versamid 973 solution (BASF) dissolved in pentanol, mixed with an additional 2.72 g of pentanol. Soft PDMS Ink: SE1700 (Dow-Corning) with 1:25 curing agent based ratio was applied for cantilever covers, micro-pins and micro-wells. Rigid PDMS ink: SE1700 (Dow-Corning), with 1:10 curing agent weight ratio, mixed 1:5 wt:wt with Sylgard 184 1:10 curing agent weight ratio (Dow-Corning) is used for wells and covers, or as gasket adhesive below PLA or ABS wells and covers.

**Print procedure with integrated profiling.** Printing was carried out using a three-axis motion-controlled stage (Aerotech) with four independent z-axes. Prior to printing, a custom automation system was applied to determine the substrate topology and relative x–y–z nozzle positions using an integrated laser profilometer, three CCD micrometers (Keyence), and custom machined fixtures. G-code generation and custom automation scripts were programmed using open-sourced Python libraries (Mecode). Extrusion was carried out using syringes, dispense tips, and a digital pneumatic regulator (EFD). Dispense tip diameters: TPU ink: 100 μm, CB:TPU ink: 200 μm, Ag:PA ink: 250 μm, Soft PDMS ink: 30 μm, Rigid PDMS ink: 410 μm. For dextran ink a refillable contact-pressure sensitive pen (0.7 mm tip, Montana) was utilized as deposition nozzle.

**Device cell seeding and culture.** Prior to cell seeding, devices were sterilized by ultraviolet–ozone exposure for 8 min. Subsequently, wells were incubated with a 50 μg ml<sup>-1</sup> solution of fibronectin (BD Biosciences) in PBS for 1 h. Fibronectin solution was aspirated and wells seeded with either primary NRVMs at a seeding density of 140 k cm<sup>-2</sup> in 10% FBS in media 199 (Life Technologies) or hiPS-CMs (Cor4U, Axiogenesis) at 220 k cm<sup>-2</sup> in designated Commercial Cor4U media (Axiogenesis). Cor4U cells were tested for mycoplasma contamination by the supplier prior to shipment. Authentication was achieved with puromycin-mediated positive selection, as described in the Supplementary Information. For thicker tissue version, NRVM are seeded at 1 M cm<sup>-2</sup> adding cold BD Matrigel (BD Biosciences) to final concentration 0.45–0.6 mg ml<sup>-1</sup>, thus below the gelling concentration. NRVMs were acquired from Sprague Dawley rats ( $n \geq 10$ , per harvest), applying procedures approved by the Harvard University Animal Care and Use Committee, described in detail in Supplementary Information. hiPS-CMs were thawed, pre-plated and seeded following guidelines from supplier, as detailed in the Supplementary Information. Cell media was changed at least every second day, applying 2% FBS in media 199 (Life Technologies) for NRVM culture, and designated Cor4U media for hiPS-CM culture.

**Data acquisition.** Data collection was performed using a custom-machined holder connecting the device to a Keithley Multichannel DMM 3706a. Readouts were obtained as two-wire resistance recordings sampling at  $\geq 60$  Hz. A custom MATLAB (MathWorks) code was applied for quantifying relative resistance changes upon tissue contraction, applying peak detection and comparison with local baseline. For electrically paced samples, a median filter (5 data points) was applied. Linear conversion constants between relative resistance change, cantilever

curvature and stress generated by tissue, were established using the designated mechanical model.

**Isoproterenol and verapamil cumulative drug-dose studies.** Cumulative dosing of isoproterenol or verapamil (Sigma-Aldrich) cardiac drugs was performed on laminar NRVM and hiPS-CM tissues inside an incubator. 700 μl serum-free media was added to each well prior to drug-dose experiments. A dilution series of the drugs in media (Life Technologies) was sequentially added in 7 μl doses. Tissue was incubated for 10 min for each dose, prior to recording. For each dose at least 30 s were recorded per channel. Isoproterenol stocks were kept at 4 °C prior to dosing. Pacing was applied using custom platinum wire electrodes. Each  $n$  denotes separate device wells with isolated tissue, sensor and media.

**Tissue immunostaining and structural analysis.** All immunocytochemistry procedures were conducted at room temperature. Samples were first fixed with 4% PFA/PBS (v/v) solution for 15 min and then permeabilized with 0.05% Triton-X/PBS (v/v) solution for 10 min. Subsequently, samples were incubated for 1 h with a monoclonal sarcomeric  $\alpha$ -actinin (clone EA-53; Sigma-Aldrich) primary antibody, washed three times in PBS, and finally counterstained with Alexa Fluor 488-conjugated anti-mouse secondary antibody, Alexa Fluor 633-conjugated Phalloidin and DAPI (Invitrogen). Samples were imaged using confocal microscopy, acquiring projected z-stack images of the wavy laminar tissues. The alignment and overall spatial organization of  $\alpha$ -actinin positive structures in the immunostained digital images were evaluated with custom MATLAB (MathWorks) code, as previously described<sup>19</sup>.

**Optical mapping experiments to determine tissue electrophysiology.** AP propagation velocities for the engineered NRVM cardiac tissues were monitored using a modified tandem-lens microscope (Scimedia) equipped with a high-speed camera (MiCAM Ultima, Scimedia), a plan APO 1X objective, a collimator (Lumencor, Beaverton, OR) and a 200 mW Mercury lamp (X-Cite exacte, Lumen Dynamics). After four days culture *in vitro*, 10 mm × 10 mm engineered laminar NRVM tissues were incubated with a 4 μM solution of a photovoltaic dye, RH237 (Invitrogen), for 5 min at 37 °C, and rinsed with Tyrode's solution prior to recording. Recordings were acquired at a frame rate of 200 Hz. Electrical point stimulation was applied to the corner of the tissue using two U-shaped platinum electrodes (Sigma-Aldrich) located 0.5–1 mm above the tissue, applying 1–2 Hz, 5–10 V pulses of 10 ms duration using a pulse generator (MyoPacer Cell Stimulator, IonOptix). Post-processing of data was conducted with custom MATLAB (MathWorks) code, as previously described<sup>21</sup>. A spatial filter with 3 × 3 pixels was applied to improve the signal-to-noise ratio. Activation time was calculated as the average time to maximum upstroke slope of pulses when continuously paced at 2 Hz during a 5 s recording window.

**Statistical analysis.** For analysis of tissue SPD, OOP and sarcomeric length, one-way analyses of variance between the compositional groups were conducted using SigmaPlot (v12.0, Systat Software Inc.). All data sets passed Shapiro–Wilk normality tests and equal variance tests. For pairwise comparison, the Holm–Sidak method was applied. For all statistical analyses,  $p$ -values less than 0.05 were considered statistically significant. Sample sizes were chosen on the basis of previous studies applying muscular thin-film assays<sup>19–21</sup>.

**Code availability.** Custom MATLAB scripts for signal detection and stress calculation can be found in the Supplementary Information.